MATERIALE PLASTICE
https://revmaterialeplastice.ro
https://doi.org/10.37358/Mat.Plast.1964

The Influence of the Delamination Location on the Bending Behavior of E-Glass Fiber EWR Flat Plates

ELENA-FELICIA BEZNEA[1], NICUSOR BAROIU[2*], IONEL CHIRICA[3]
[1]Dunarea de Jos University of Galati, Faculty of Engineering, Department of Mechanical Engineering, 111 Domneasca Str., 800008, Galati, Romania, ORCID iD: 0000-0001-8398-7055
[2]Dunarea de Jos University of Galati, Faculty of Engineering, Department of Manufacturing Engineering, 111 Domneasca Str., 800008, Galati, Romania, ORCID iD: 0000-0002-1334-7025
[3]SDG - Ship Design Group, 1A Luminoasa Str., 807325, Vanatori, Galati, Romania

Abstract: *The paper presents a study on the stresses and deformations induced by the transversal loading of some flat plates made of E Glass EWR Fiberglass Woven Roving type, having delamination type defects. The parametric analysis of the delamination influence on the stresses and displacements occurring in the plate material is performed. The results of the static calculation are compared with the experimental tests of the flat plates subjected to bending, highlighting the concordance of the variation of the stresses and displacements versus to the delamination position.*

Keywords: *composite materials, E-Glass fiber, static analysis, FEM analysis, delaminations sandwich*

1. Introduction

E-Glass fiber EWR is a material made of e-glass direct roving by plain/twill weaving style. This is widely applied to FRP (fiber reinforced polymer) boat, surfboard, tank, panel as well as other FRP products. Due to necessity to reduce the fuel consumption - the current trend in the field of automotive, railways, aviation or aerospace - the use of composite materials is much broader. In the marine field [1, 2], multiple applications have been developed, where polymer matrix and reinforcing material are used for various structural components. This fact leads to the decreasing of the total weight, and implicitly to the fuel consumption, doubled by the increase in the cruise speed [3-5]. Composites have many special characteristics: high strength-to-weight ratios much higher than in classical materials (metals, wood etc.) (one of the biggest advantage); so they are easy, due to the low densities [6–8]; have high fatigue strength [9,10], good resistance to corrosion of environmental factors or other corrosive agents [11, 12]; easier to be produced (the technologies for forming parts from these materials are relatively simple in number of operations and have low energy consumption); high vibration damping capacity [11-13]; increased durability and high safety in operation (breaking a fiber from a composite piece does not lead to the damage of the whole part); chemical stability and high resistance to high temperatures [14-16]; good mechanical stability [17-20]; high insulating properties etc.

The determination as close to reality as possible of the behavior of the thin, ultralight and highly strength composite structures required for bending, involves elements of theoretical numerical analysis [21, 22], analysis by the method of finite elements [23-25], or experimental analysis [26-28]. Obviously, the behavior of such structures is correlated with the thickness of the walls, the configuration of the stiffening, the angle of arrangement of the fibers or the type of load applied [29-32]. The introduction of fibers or other reinforcing elements in the matrix of stratified composite materials, depending on the characteristics and conditions of use of the product, aims to obtain materials with high strength compared to the organic matrix used as a basis.

The placement of the fibers in the layers or groups of layers is performed according to the mechanical performances pursued for the structure made of the certain material (stiffness, strength). Practically, by an appropriate structural design, the lifetime of a layered composite can be considerably extended, precisely due to the configuration and the reduced number of elastic constants by which they are characterized.

**email: Nicusor.Baroiu@ugal.ro*

Finite element parametric studies on the stress concentration factors (SCF) in tubular X connections equipped with fiber reinforced polymer (FRP) under out-of-plane and in-plane bending moment, experimentally validated, were performed, which demonstrated the effect of FRP and connection geometry on the SCFs, showing that an increase in the number of FRP sheets causes a notable decrease in the SCFs [33, 34].

In determining the best characteristics for various composite structures, instruments for the analysis of large volumes of theoretical or experimental data, such as artificial neural networks, can be used, for which suitable models can be found [33, 34].

Due to operational loading, damage may occur by delamination, by interlaminar cracking and breaking [35-38]. In these conditions, the analysis of their effects on the performances of the structure, is an important stage of the design of the laminated composite plates [39-44].

Delaminations lead to effects such as reducing the ability to take over static and, above all, dynamic loads, such as those resulting from impact; the introduction of additional buckling modes, the sublaminations that are occuring during the buckling at much loads; modification of natural frequencies and vibration modes etc. Cracking by local delaminations can be detected by non-destructive processes, but expensive sometimes.

That is why the analysis of the phenomena of occurring possible delaminations, as well as their effects on the performance of the structure, is an important step in designing the configurations of laminated composite boards.

2. Materials and methods

The material used for plate fabrication is Roving EWR with polyester resin, with the following characteristics:

- Young's moduli and shear moduli

E_x = 38.6 GPa, E_y = 38.6 GPa, E_z = 8.27 GPa, G_{xy} = 4.1 GPa, G_{yz} = 4.1 GPa, G_{zx} = 4.1 GPa,

- Poisson's ratios

$$\mu_{xy} = 0.26;\ \mu_{yz} = 0.26;\ \mu_{xz} = 0.26.$$

The orientation of the fibers in the layers is shown in Figure 1.

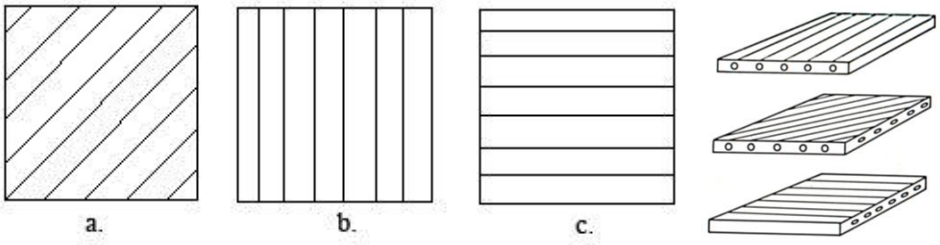

Figure 1. Theoretical model of fibers oriented, towards the plate axis:
a. - fibers oriented at +45°; b. - fibers oriented at +90°; c. - fibers oriented at 0°

Fabrication stages for obtaining a layered composite panel

The stages of manufacture of composite type panels are: textile tailoring of the layers, Figure 2 and Figure 3; in a container, the polyester resin is prepared by adding the specific hardening agent.

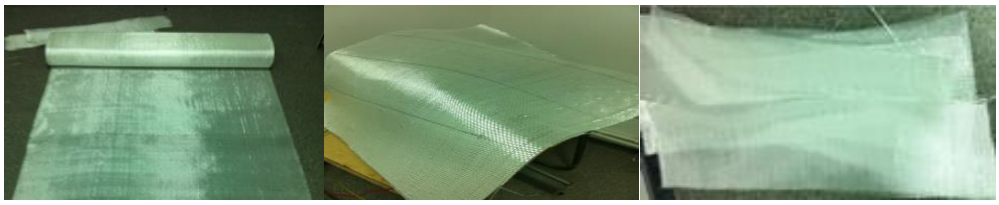

Figure 2. The textile tailoring

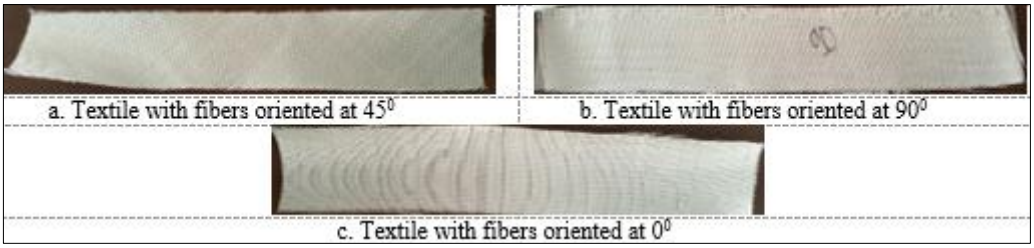

Figure 3. Practical fiber orientation model

Flat, rectangular layered composite plates with a length L = 600 mm, width l = 100 mm and thickness h = 4 mm have been performed. The plates have six macrolayers, arranged symmetrically on the thickness, relative to the median plane.

Experimental determination of the displacements of flat plates made of composite materials, in bending

The shape of the delamination area has been considered as elliptical one. The studies on the static bending behavior of the plates made of layered composite materials were focused so on the perfect flat plates and on imperfect plates (with elliptical central delamination). Four cases have been treated. In Table 1, the positions of the delaminations of the elliptical imperfection (50 mm x 12.5 mm) are shown.

Table 1. Plates with central elliptical delaminations (cases *a*, *b* and *c*)

Case *a* (ellipse axes oriented at 0⁰)	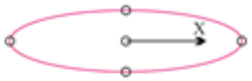
Case *b* (ellipse axes oriented at 45⁰)	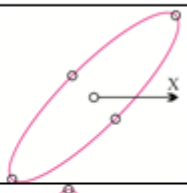
Case *c* (ellipse axes oriented at 90⁰)	
Perfect plate	

The position of delamination was considered to be placed between two neighboring macrolayers, *S1-S2*, *S2-S3*, *S3-S4*, *S4-S5*, *S5-S6*, Table 2. A macrolayer is a group of adjacent layers, having the same characteristics. Topological code of the composite plate is $[90_2/45_1/0_2]_S$.

Table 2. Position of the layers

Macro-layer	º [degree]	Number of layers	h [mm]
S1	90	2 layers	0.8
S2	45	1 layer	0.4
S3	0	2 layers	0.8
S4	0	2 layers	0.8
S5	45	1 layer	0.4
S6	90	2 layers	0.8

For the experiments, four plates of the layered composite have been considered: the perfect plate and the plate with all types of delaminations located between *S1-S2* (Figure 4).

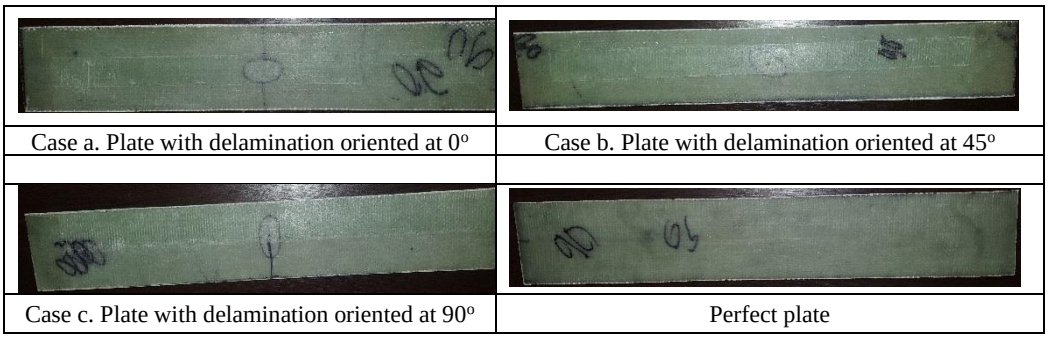

Case a. Plate with delamination oriented at 0º | Case b. Plate with delamination oriented at 45º

Case c. Plate with delamination oriented at 90º | Perfect plate

Figure 4. Plates fabricates for the three cases of delaminations

The loading has been provided by the weights. For displacement measuring transducers type LVDT 300 mm with strain gauge bridge type Quantum, laptop and acquisition software and data analysis (Catman) have been used (Figure 5).

a. Transducer balancing | b. Test device

Figure 5. Experimental setup

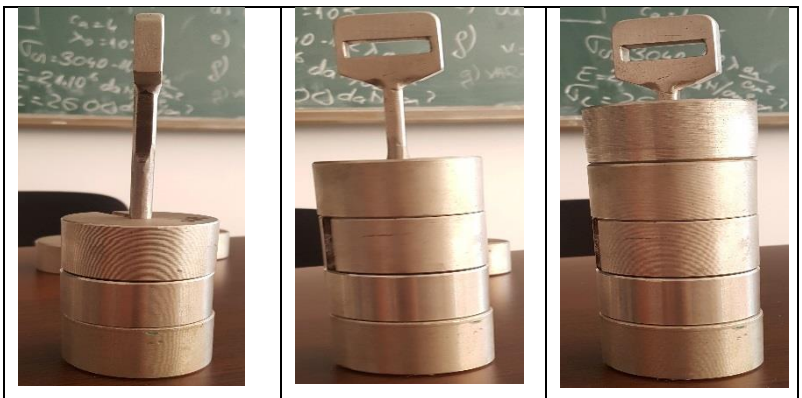

a. The mass m_1 | b. The mass m_2 | c. The mass m_3

Figure 6. Loading masses for the loading

The plates have been simple supported on the short sides, at 10 mm away from the ends. Progressive masses have been considered as loading for each plate (m_1 = 2.77 kg; m_2 = 3.66 kg; m_3 = 4.55 kg), Figure 6. For each loading, the transversal displacement in the middle section (for all plates) has been recorded.

FEM study of the bending of composite plane plates having delaminations

The FEM analysis has been performed with package COSMOS-M. The layered plates with thickness of 4 mm, simply supported at 10mm from the ends have been loaded by an evenly distributed pressure *p* (p_1 = 0.00543474 MPa, p_2 = 0.00718092 MPa and p_3 = 0.0089271 MPa) on an surface of 100 mm x 50 mm. The loading has been provided by the masses m_1, m_2 and m_3. The both areas of the plate (perfect area and delaminated area) have been modeled as layered material:
- the perfect area has been modeled with elements type SHELL3L, having six macrolayers;
- the delaminated area have been modeled as two overlapping plates, being in contact.

On the delaminated area outline continuity conditions for displacements have been imposed. The corresponding points of the contact areas of the delamination (upper and lower) are imposed to have the same displacements. The length of the elements is taken as 10 mm, and only the linear behavior of the material was taken into account. The total number of elements of the mesh of plate *a* is 1242 elements; the total number of elements of the mesh of plate *b* is 1250 elements; the total number of elements of the mesh of plate *c* is 1248 elements, and the total number of elements of the mesh plate *d* is 1220 SHELL3L elements, Figure 7.

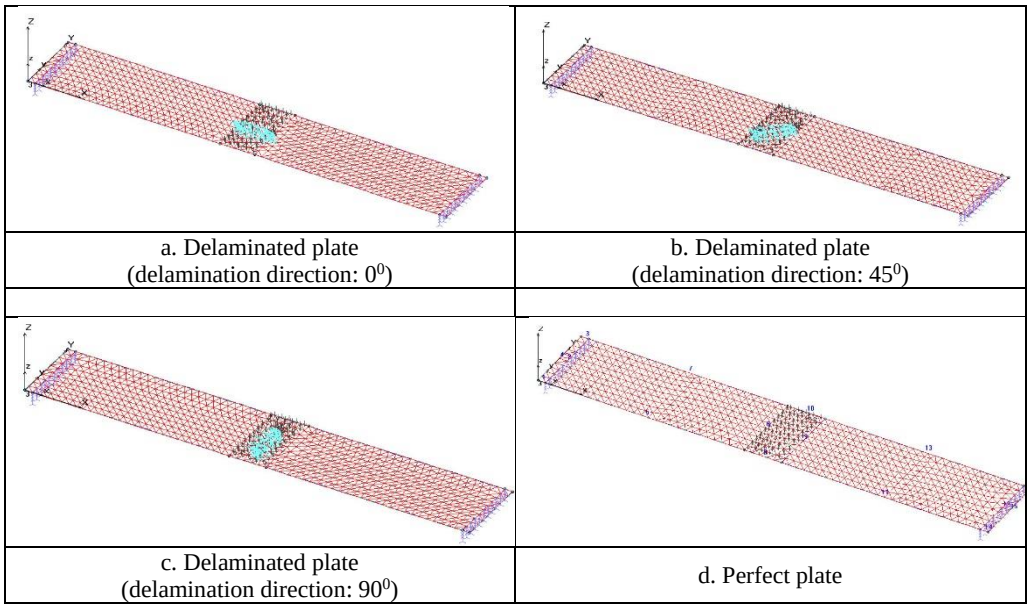

a. Delaminated plate (delamination direction: 0^0)

b. Delaminated plate (delamination direction: 45^0)

c. Delaminated plate (delamination direction: 90^0)

d. Perfect plate

Figure 7. Mesh of the layered composite plates

3. Results and discussions

Bending behavior of the plates made of composites, having delaminations - FEM calculus

According to Theory of Elasticity, a thin plate means a plate with small thickness versus the other dimensions, having also small deformations versus the thickness (generally speaking, the deformations are not greater than thickness). The deformations of the anisotropic plates are characterized by the fact that the average surface after deformation remains flat. The plate bending is given by the external loading acting on the surface, normal to the median plane before the deformation and by bending moments and normal forces acting on the median plane, distributed on the outline. The forces may be the reactions in the case of simply supported outlines. The *xy* plane is considered to be the median plane of the non deformed plate, and the *z*-axis is normal to the non deformed median plane.

Figure 8 shows the map of the displacements of the perfect plate acting by pressures p_1, p_2 and p_3.

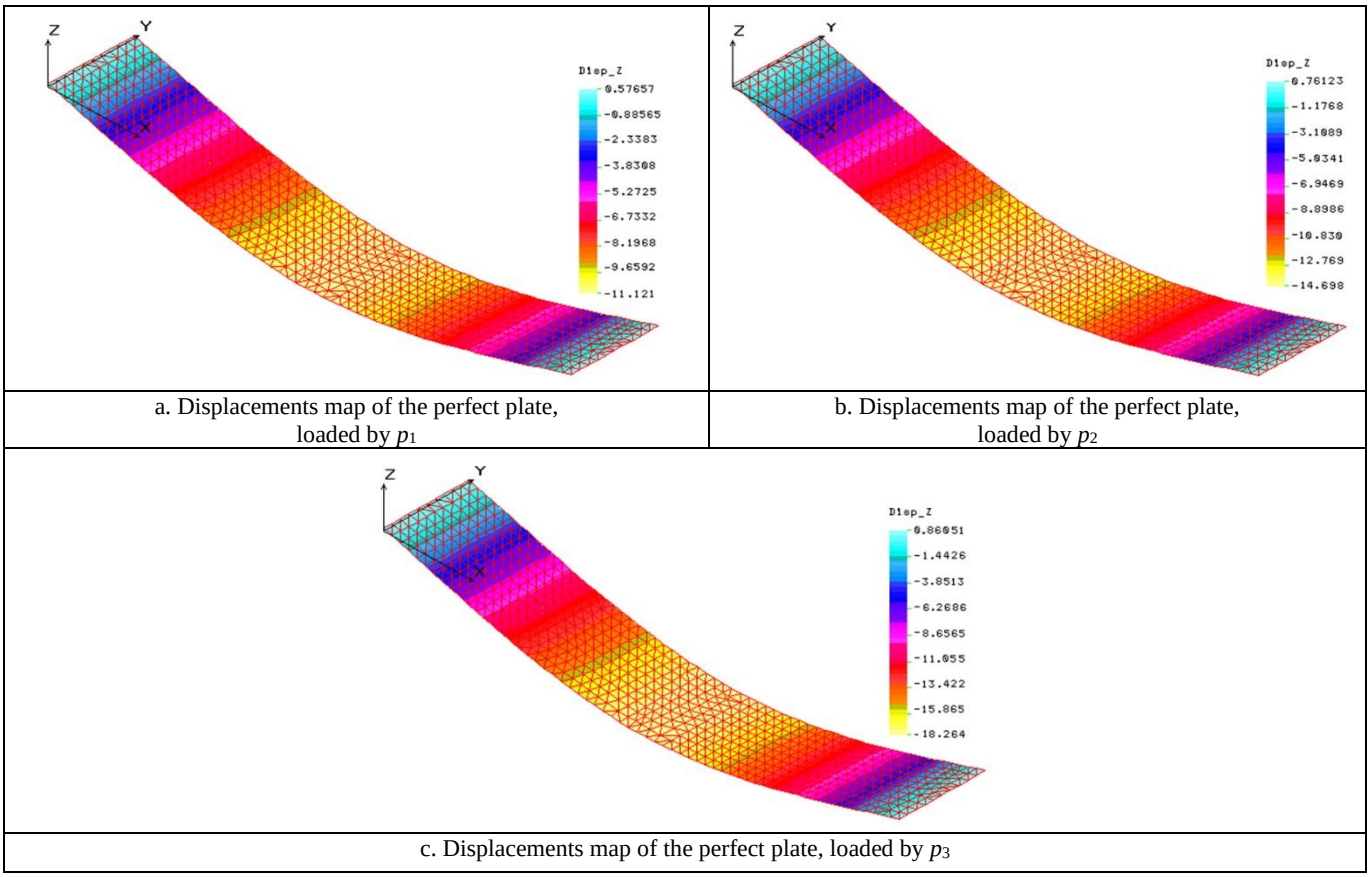

a. Displacements map of the perfect plate, loaded by p_1

b. Displacements map of the perfect plate, loaded by p_2

c. Displacements map of the perfect plate, loaded by p_3

Figure 8. Displacements map of the perfect plate

For the studied cases (the plate with the delamination oriented at 0º - Case *a*; the plate with the delamination oriented at 45º - Case *b*; the plate with the delamination oriented at 90º - Case *c* and the perfect plate), loaded by p (p_1, p_2 and p_3), given by the masses m_1, m_2 and m_3, for the six macrolayers (*S1-S2; S2-S3; S3-S4; S4-S5* and *S5-S6*), the values of the resulted displacements are presented in Table 3.

Table 3. Displacements [mm] obtained in the analysed cases - FEM calculus

Macro-layers	p [MPa]	Perfect	Case *a*	Case *b*	Case *c*
S1-S2	p_1	11.12	12.48	11.13	12.57
	p_2	14.69	16.49	14.7	16.61
	p_3	18.26	20.5	18.27	20.65
S2-S3	p_1	11.18	12.55	11.21	12.57
	p_2	14.77	16.58	14.81	16.61
	p_3	18.36	20.61	18.41	20.65
S3-S4	p_1	11.22	12.60	11.30	12.57
	p_2	14.83	16.64	14.93	16.61
	p_3	18.43	20.69	18.56	20.65
S4-S5	p_1	11.21	12.58	11.21	12.57
	p_2	14.81	16.62	14.81	16.61
	p_3	18.41	20.66	18.41	20.65
S5-S6	p_1	11.17	12.48	11.13	12.57
	p_2	14.76	16.49	14.70	16.61
	p_3	18.35	20.5	18.27	20.65

The variation of maximum displacements w_z (in mm) versus the position of the delaminations on the layers, for loading the plates with the pressure p (p_1, p_2 and p_3), respectively the variation of maximum

displacements versus the position of the delamination relative to the plate surface, for loading the plates with p (p_1, p_2 and p_3) are graphically presented in Figures 9÷11.

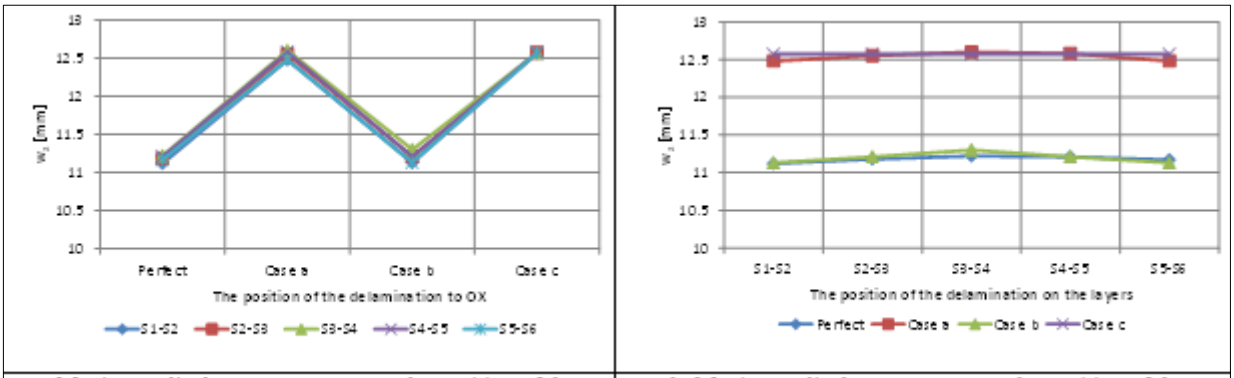

a. Maximum displacements w_z versus the position of the delaminations on layers, for loading p_1

b. Maximum displacements versus the position of the delamination relative to axis OX, for loading p_1

Figure 9. Variation of maximum displacements versus position of the delamination on layers and versus position relative to OX for loading p_1

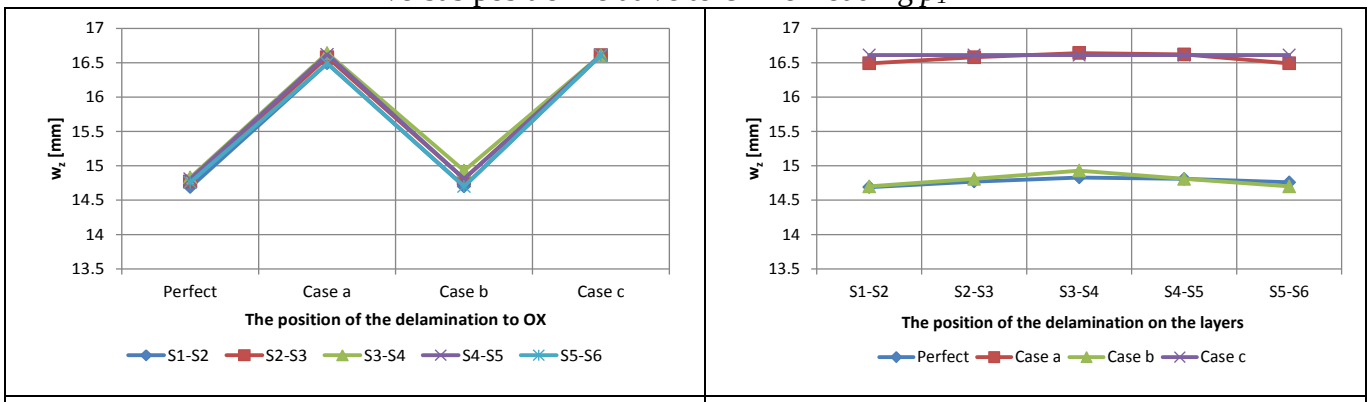

a. Maximum displacements w_z versus the position of the delaminations on layers, for loading p_2

b. Maximum displacements w_z versus the position of the delamination relative to axis OX, for loading p_2

Figure 10. Variation of maximum displacements versus position of the delamination on layers and versus position relative to OX for loading p_2

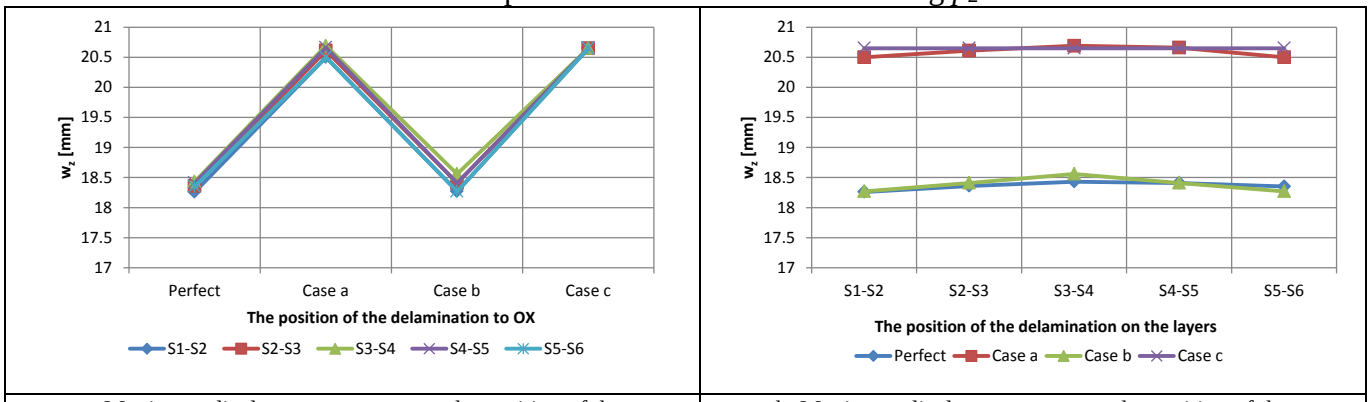

a. Maximum displacements w_z versus the position of the delaminations on layers, for loading p_3

b. Maximum displacements versus the position of the delamination relative to axis OX, for loading p_3

Figure 11. Variation of maximum displacements versus position of the delamination between layers and versus position relative to OX axis for loading p_3

Figure 12 shows the variation of maximum displacement versus the position of the delamination on the layers, for loading with all pressures (p_1, p_2 and p_3). Figure 13 shows the variation of maximum

displacement versus the position of the delamination relative to axis *OX*, for loading with all pressures (p_1, p_2 and p_3).

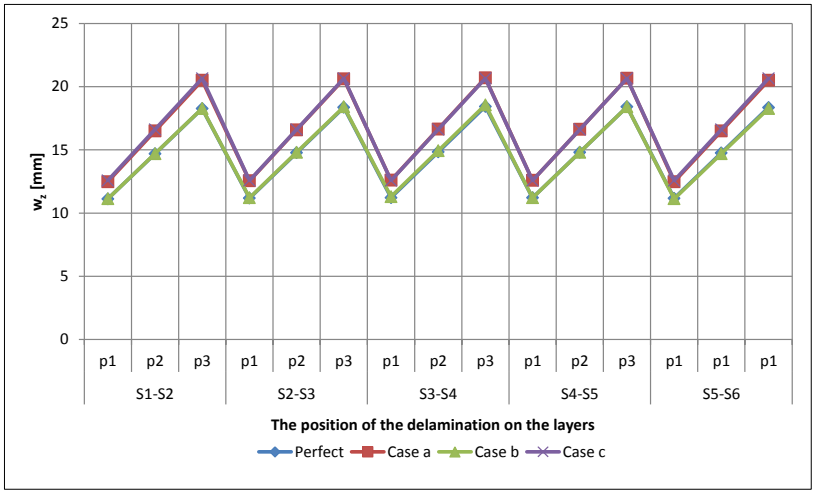

Figure 12. Variation of maximum displacement versus the position of the delamination on the layers, for loading with all pressures p_1, p_2 and p_3

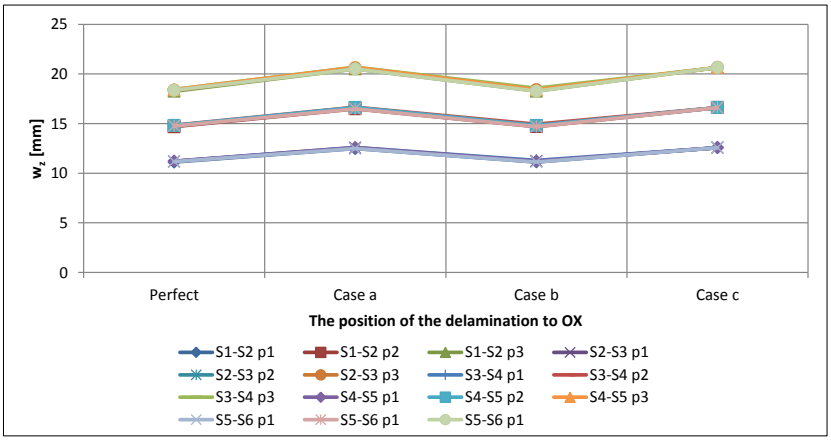

Figure 13. Variation of maximum displacement versus the position of the delamination relative to axis *OX*, for loading with all pressures p_1, p_2 and p_3

Bending behavior of the plates made of composites, having delaminations - Experiments

In Table 4, the values of maximum displacements obtained by experiments are shown - (plate with delamination oriented at 0^o - Case *a*; plate with delamination oriented at 45^o - Case *b*; plate with delamination oriented at 90^o - Case *c* and perfect plate), under the action of pressure *p* (p_1, p_2 and p_3), given by the masses m_1, m_2 and m_3 for two macrolayers (*S1-S2* and *S5-S6*). The four cases are the same as in FEM calculus.

Table 4. Maximum displacements [mm] obtained in experiments

Macro-layers	*p* [MPa]	Perfect	Case *a*	Case *b*	Case *c*
S1-S2	p_1	13.18	14.21	13.81	14.29
	p_2	16.87	18.99	16.57	18.64
	p_3	20.3	22.75	20.04	22.15
S5-S6	p_1	13.1	13.87	13.97	14.29
	p_2	17.13	18.72	16.35	18.64
	p_3	20.42	22.85	20.13	22.15

Figures 14÷15 show the variation of maximum displacements w_z (in mm) versus the position of delaminations on layers, for loadings with pressure *p* (p_1, p_2 and p_3), respectively variation of

displacements versus position of delamination relative to axis *OX*, for loading *p* (p_1, p_2 and p_3). The comparations between FEM analysis (*C*) and experiments (*E*) are shown.

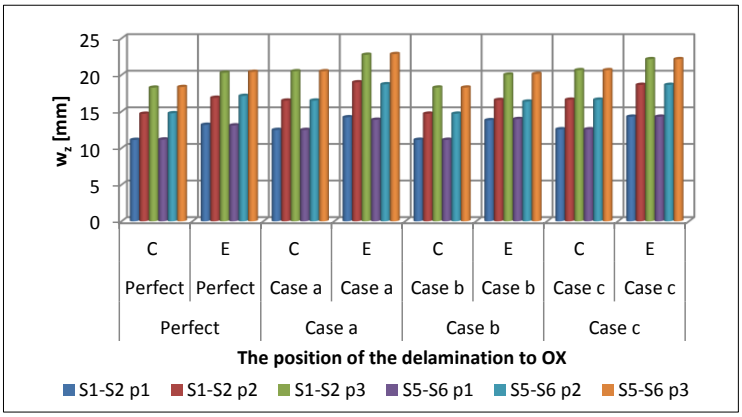

Figure 14. Variations of maximum displacements versus position of delamination relative to *OX* axis for loading with pressures p_1, p_2 and p_3 (FEM analysis - *C* and experiments - *E*)

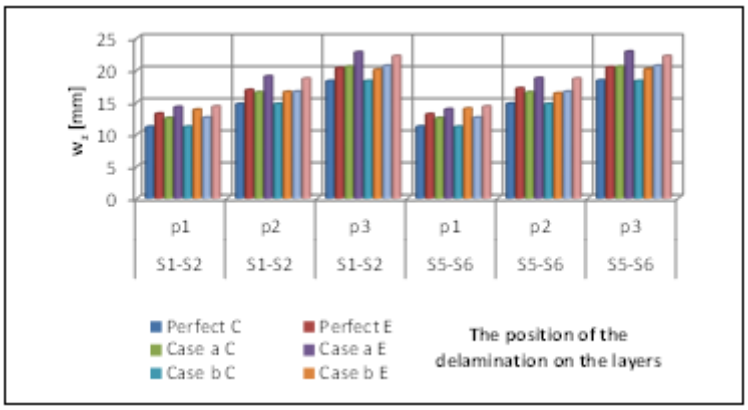

Figure 15. Variations of maximum displacements versus position of delamination on layers, for loading with pressures p_1, p_2 and p_3 (FEM analysis - *C* and experiments - *E*)

For the pressure values p_1, p_2 and p_3, in defining the displacement relative to the delamination position relative to the *OX* axis, respectively the displacement relative to the delamination position on the layers, the results obtained experimentally, compared to those obtained by FEM analysis, are shown in Figures 16÷18, for macrolayers *S1-S2* and *S5-S6*.

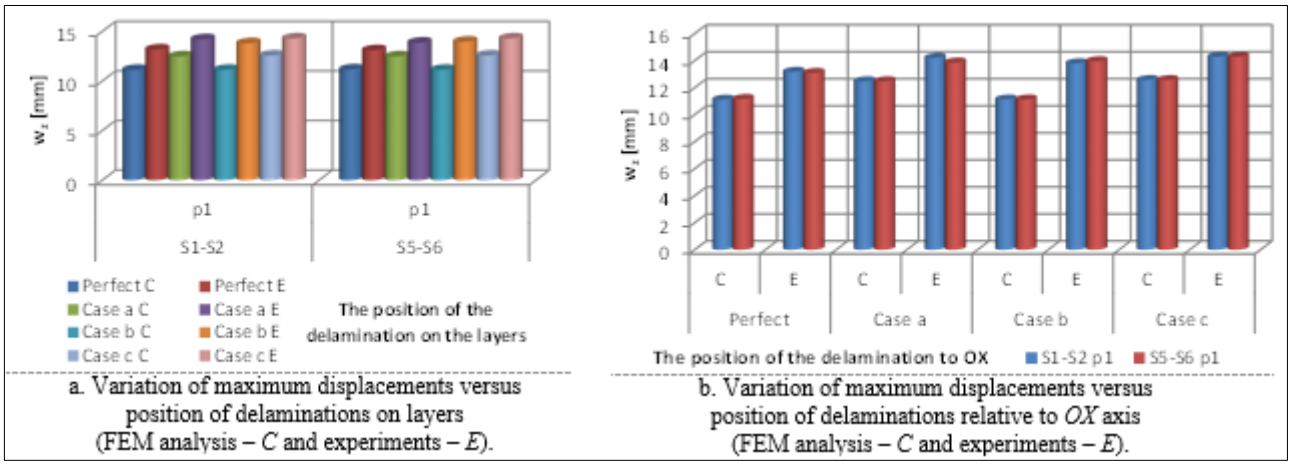

a. Variation of maximum displacements versus position of delaminations on layers (FEM analysis – *C* and experiments – *E*).

b. Variation of maximum displacements versus position of delaminations relative to *OX* axis (FEM analysis – *C* and experiments – *E*).

Figure 16. Variation of maximum displacements versus position of delaminations for loading p_1

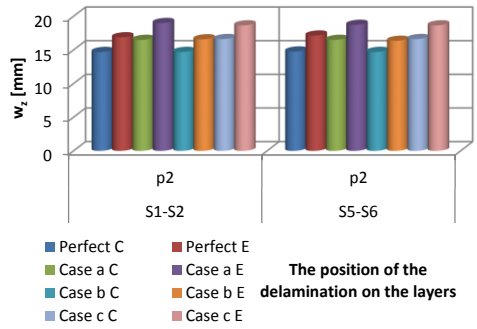

a. Variation of maximum displacements versus position of delaminations on layers (FEM analysis – *C* and experiments – *E*)

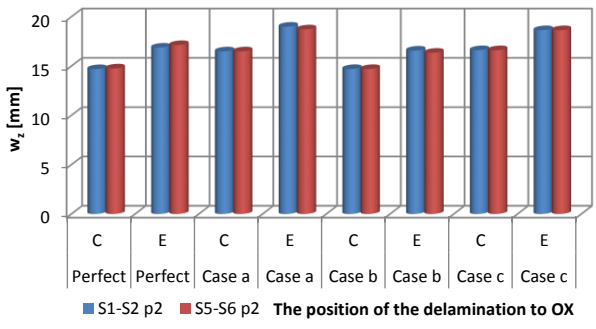

b. Variation of maximum displacements versus position of delaminations relative to *OX* axis (FEM analysis – *C* and experiments – *E*)

Figure 17. Variation of maximum displacements versus position of delaminations for loading p_2

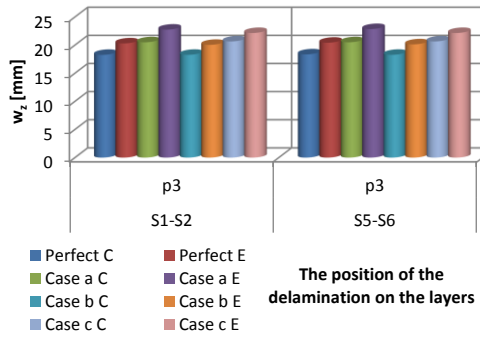

a. Variation of maximum displacements versus position of delaminations on layers (FEM analysis – *C* and experiments – *E*)

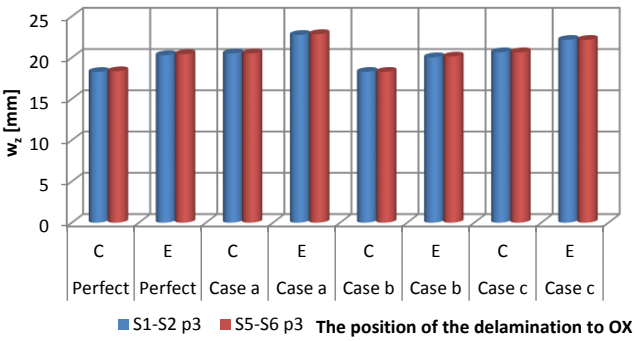

b. Variation of maximum displacements versus position of delaminations relative to *OX* axis (FEM analysis – *C* and experiments – *E*)

Figure 18. Variation of maximum displacements versus position of delaminations for loading p_3

Experimental determination of stresses and displacements

For analyzed cases (plate with delamination oriented at 0º - Case *a*; 45º - Case *b*; 90º - Case *c* and perfect plate), loaded by pressure p_3, for the six macrolayers (*S1-S2; S2-S3; S3-S4; S4-S5* and *S5-S6*), in the Tables 5÷12 the numerical values and graphical changes of normal and shear stresses through the thickness of the plate for a cross-section with and without delamination are illustrated.

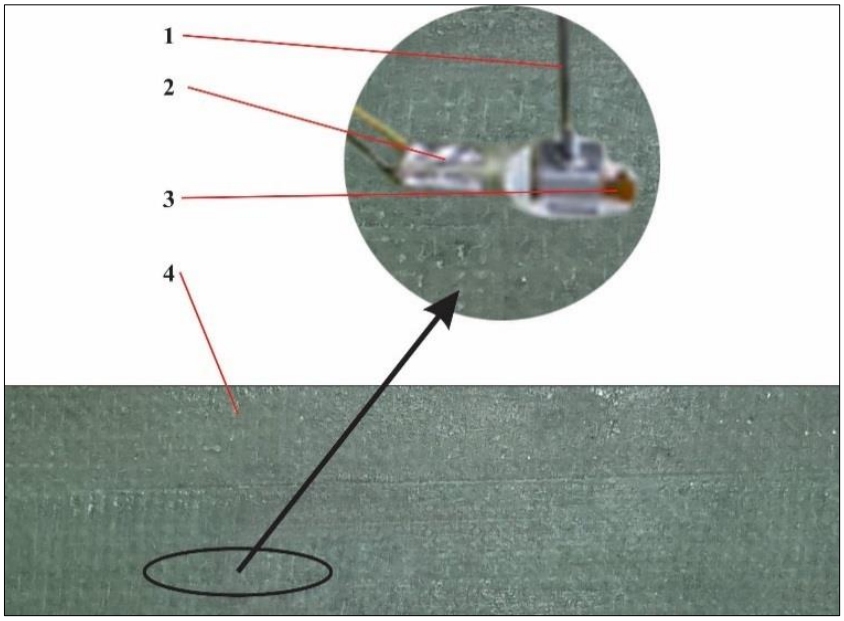

Figure 19. Experimental setup: 1 - extensometer arm; 2 - compensation strain gauge; 3 - strain gauge; 4 - specimen (plate with delamination oriented at 90^o)

The experimental rig for stress measurements is illustrated in Figure 19.

In figures from Tables 6, 8, 10 and 12, *z* axis has vertical orientation, stress axis has horizontal orientation. The numerotation of layers are from top to down of figure (that is layer 1 is positioned between z=2mm to 1.2mm; layer 2 is positioned between z=1.2mm to 0.8mm etc.).

Table 5. Normal and shear stresses (in MPa) occurred in layers for p_3 loading (plate with delamination at 0^o - Case *a*) at the interface with embedded delamination

Delamination	***p* [MPa]**		***Top***	***Bottom***	***Top***	***Bottom***
		Macrolayer	σ_x	σ_x	τ_{xy}	τ_{xy}
S1-S2	p_3	*2*	128.1	**-8.568**	-7.459	**-5.030**
		1	**-88.08**	-52.74	**-11.89**	-7.020
S2-S3	p_3	*3*	-91.6	**-0.7719**	16.4	**0.2956**
		2	**-127.**	-85.08	**-6.951**	-4.640
S3-S4	p_3	*4*	-0.0041	**15.04**	-0.00681	**-2.680**
		3	**-90.28**	-0.025	**16**	-0.0408
S4-S5	p_3	*5*	14.19	**21.21**	0.766	**1.153**
		4	**0.698**	91.60	**-0.350**	-16.40
S5-S6	p_3	*6*	8.944	**14.94**	1.282	**2.172**
		5	**86.79**	130.1	**5.437**	8.094

The gap of stresses values at interface of layers with embedded delamination are bolded.

Table 6. Variation of normal and shear stresses (in MPa) on layers for p_3 loading of plate with delamination at 0° - Case *a*

Case a Delimitation position	σ_x	τ_{xy}
S1-S2	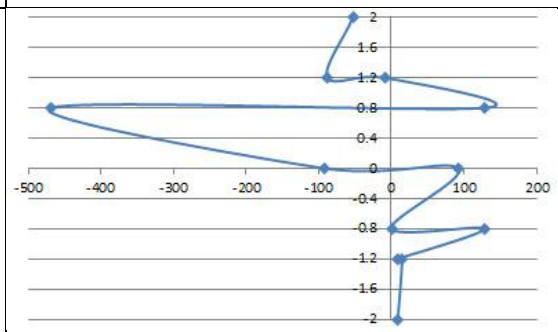	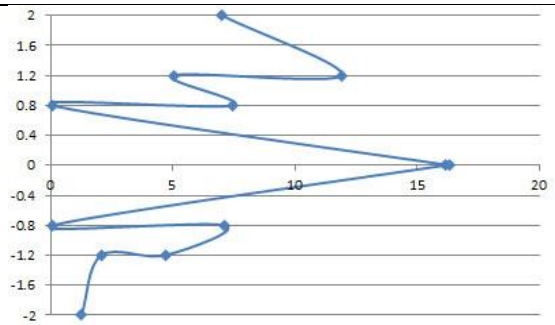
S2-S3	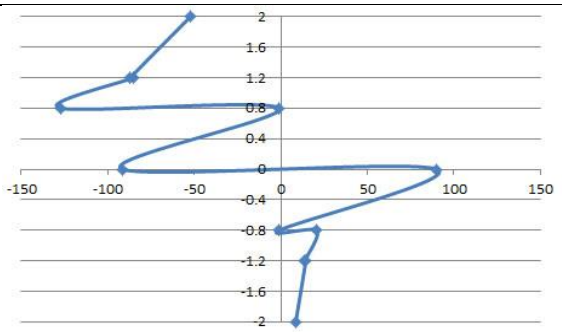	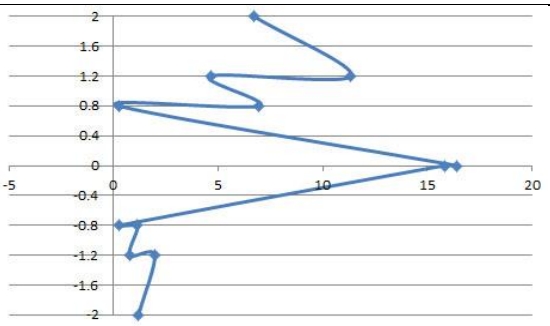
S3-S4	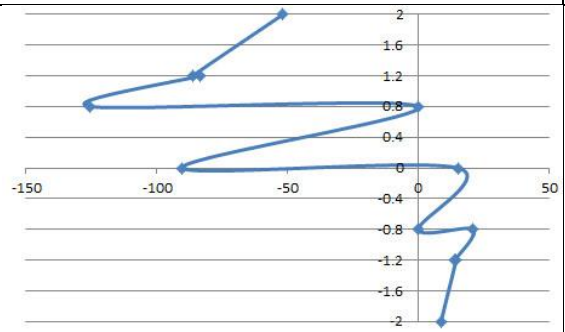	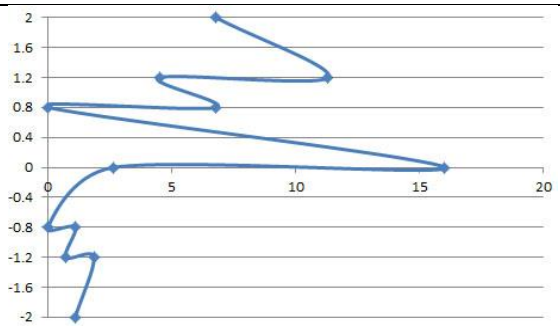
S4-S5	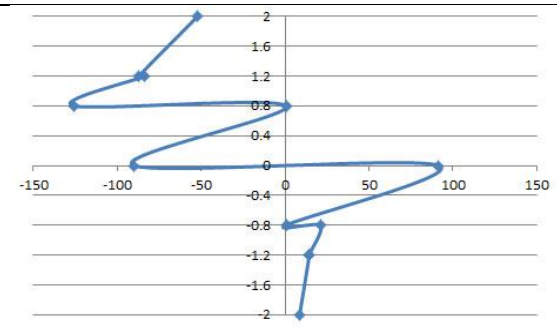	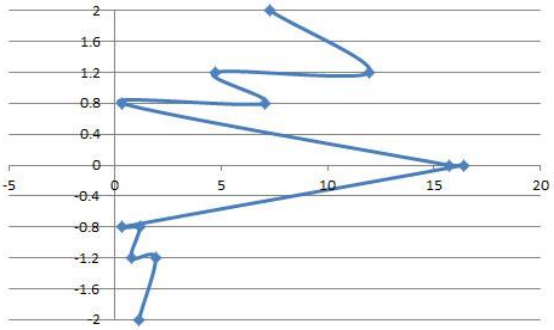

S5-S6	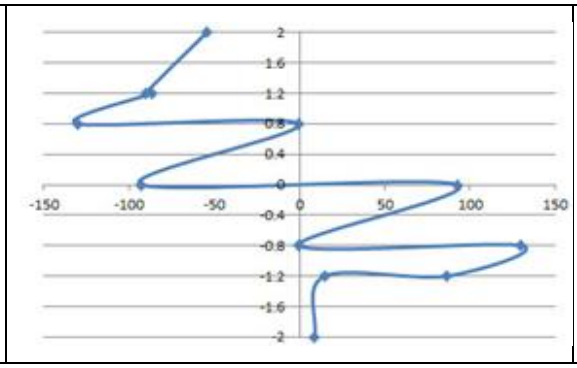	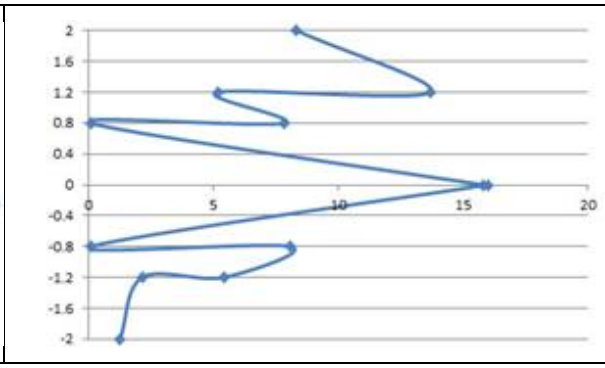

Table 7. Normal and shear stresses (in MPa) occurred in layers for p_3 loading (plate with delamination at 45° - Case *b*), at the interface whith embedded delamination

Delamination	p [MPa]		Top	Bottom	Top	Bottom
		Macrolayer	σ_x	σ_x	τ_{xy}	τ_{xy}
S1-S2	p_3	*2*	-125.1	**-83.52**	-15.62	**-10.40**
		1	**-89.4**	-53.67	**-25.52**	-15.38
S2-S3	p_3	*3*	-80.8	**0.9396**	8.21	**-0.327**
		2	**-125.1**	-83.15	**-15.87**	-10.64
S3-S4	p_3	*4*	0.002	**13.52**	-0.001	**-1.391**
		3	**-81.09**	0.0124	**8.332**	0.008
S4-S5	p_3	*5*	13.81	**20.69**	1.774	**2.649**
		4	**-0.925**	80.41	**0.324**	-8.092
S5-S6	p_3	*6*	8.945	**14.90**	2.562	**4.252**
		5	**83.5**	125.1	**10.39**	15.61

Table 8. Normal and shear stresses (in MPa) variation in layers for p_3 loading (plate with delamination at 45° - Case *b*)

Case b ***Delamination position***	σ_x	τ_{xy}
S1-S2	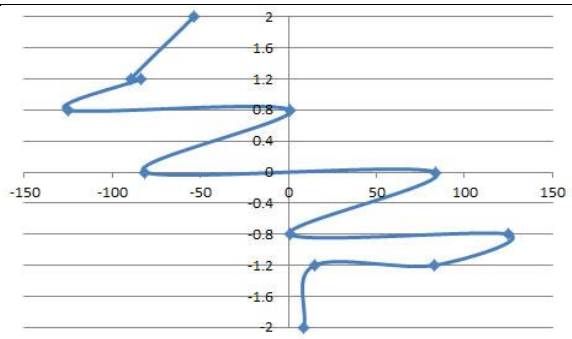	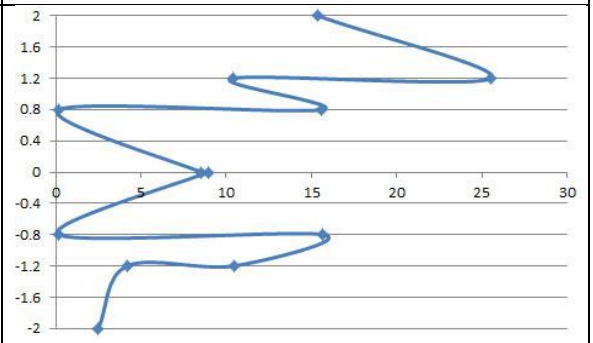
S2-S3	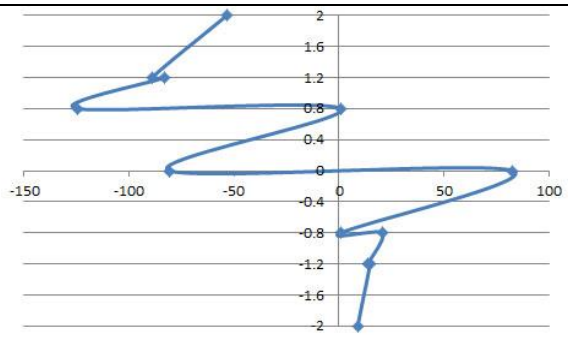	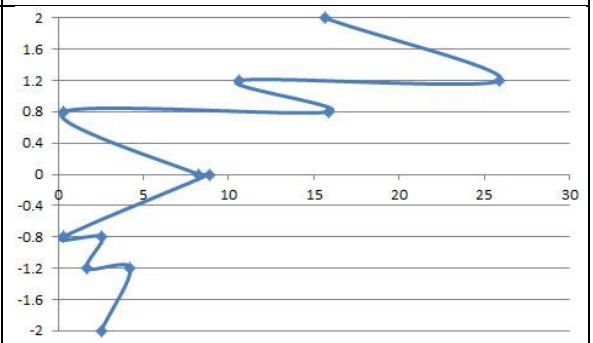

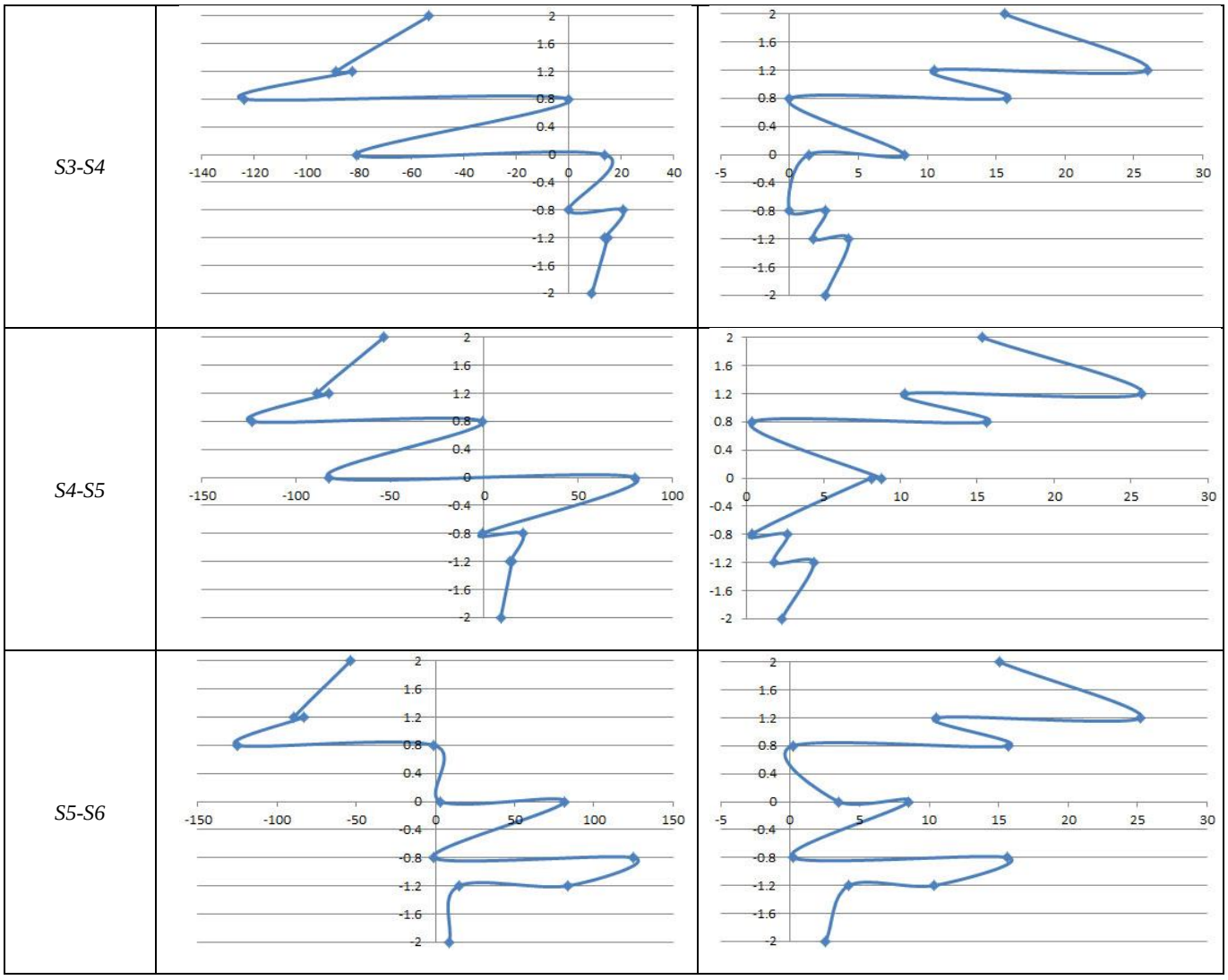

Table 9. Normal and shear stresses (in MPa) occurred in layers for p_3 loading (plate with delamination at 90° - Case *c*), at the interface whith embedded delamination

Delamination	*p* [MPa]		*Top*	*Bottom*	*Top*	*Bottom*
		Macrolayer	σ_x	σ_x	τ_{xy}	τ_{xy}
S1-S2	p_3	*2*	35.91	**23.79**	6.406	**4.119**
		1	**145.1**	86.46	**10.17**	5.867
S2-S3	p_3	*3*	26.03	**-0.4896**	-8.552	**-0.185**
		2	**35.47**	23.44	**6.476**	4.205
S3-S4	p_3	*4*	0.000007	**-4.370**	1.39E-06	**1.366**
		3	**26.22**	0.000004	**-8.197**	0.000008
S4-S5	p_3	*5*	-3.907	**-5.911**	-0.701	**-1.079**
		4	**0.490**	-26.03	**0.187**	8.552
S5-S6	p_3	*6*	-14.41	**-24.08**	-0.978	**-1.695**
		5	**-23.79**	-35.91	**-4.119**	-6.406

The changes of stresses values at interface of layers with embedded delamination are bolded.

Table 10. Normal and shear stresses (in MPa) variation in layers for p_3 loading (plate with delamination at 90° - Case *c*)

Case c Delamination position	σ_x	τ_{xy}
S1-S2	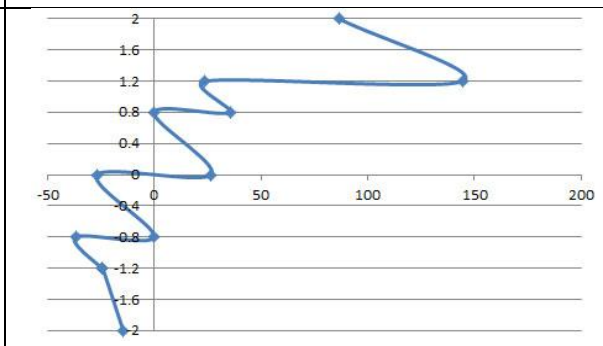	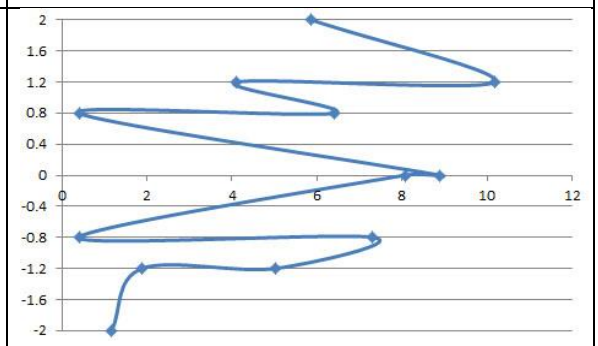
S2-S3	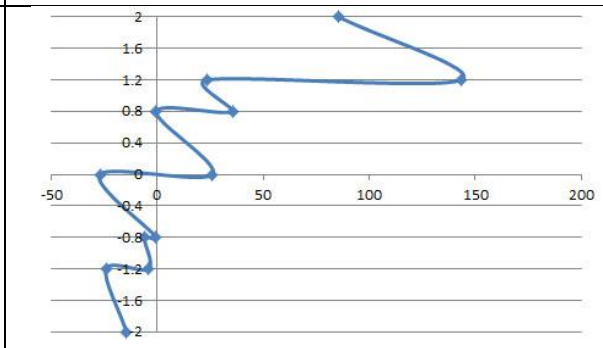	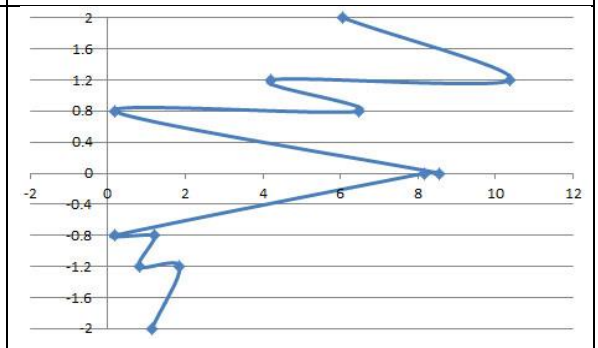
S3-S4	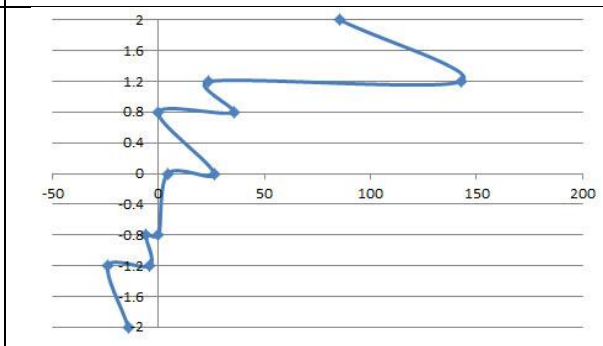	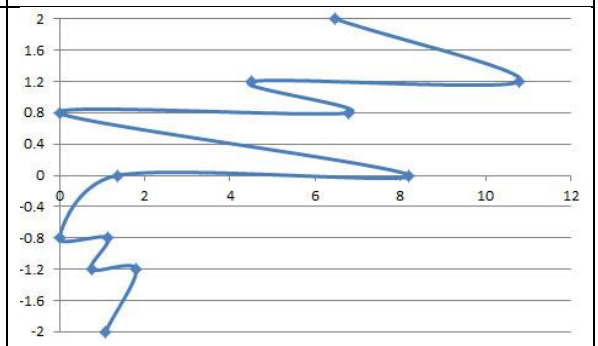
S4-S5	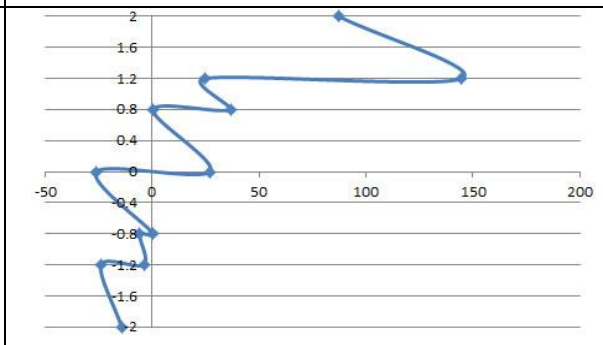	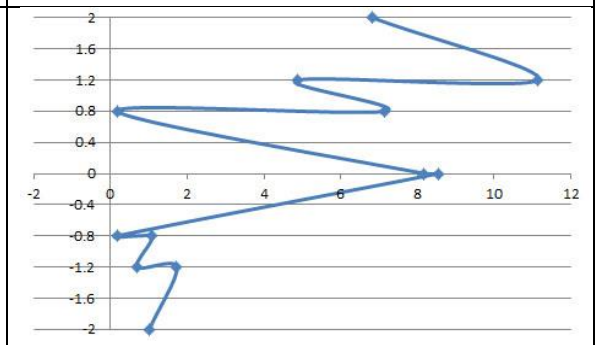

S5-S6	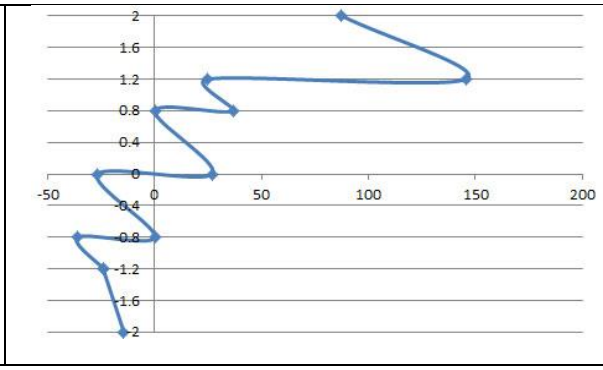	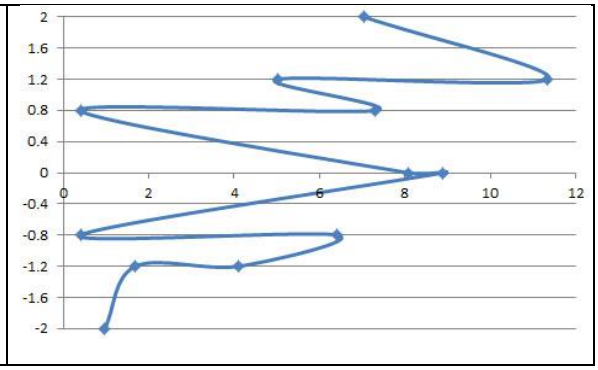

Table 11. Normal and shear stresses (in MPa) occurred in layers for p_3 loading (perfect plate)

***p* [MPa]**		***Top***	***Bottom***	***Top***	***Bottom***
	Layer	σ_x	σ_x	τ_{xy}	τ_{xy}
p_3	*1*	8.441	14.07	0.	1.705
	2	13.39	20.09	1.219	1.899
	3	-0.	13.90	1.829	2.842
	4	-13.9	-0.	2.842	1.829
	5	-20.09	-13.39	1.899	1.219
	6	-14.07	-8.441	1.705	0.

Table 12. Normal and shear stresses variation (in MPa) in layers for p_3 loading (perfect plate)

Perfect	σ_x	τ_{xy}
	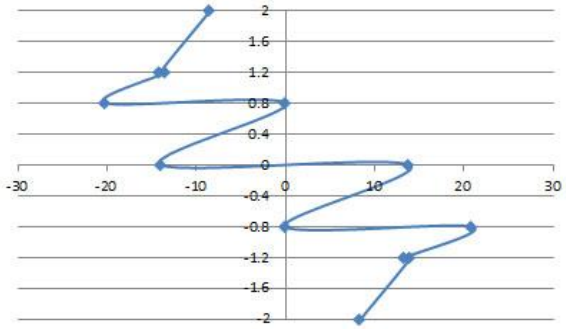	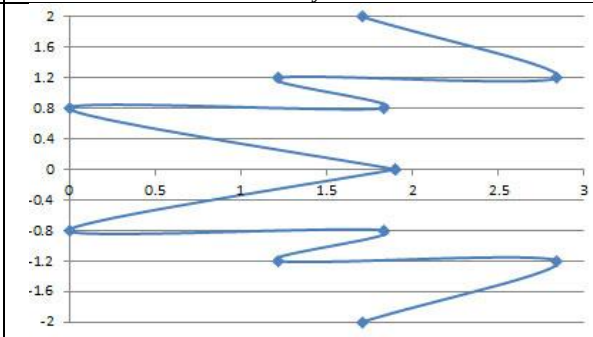

Discussions

Delamination is an important failure mechanism for layered composites due to the low interlaminar strength. The dangers of delamination phenomena are occurring due to out-of-plane loading and especially dynamic (impact) loads. Delamination can also have a major effect on in-plane failure.

In FEM calculus, certain hypotheses have been considered:

- plates are considered thin, having constant thickness. So, a two dimensional model should be approached;
- the layered composites are made of orthotropic layers, parallels and perfect bounded each others. The hypothesis of perfect assembled can be translated as the same displacement for the corresponded points placed on the layers interfaces
- the behavior of each layer is a linear elastic one;
- the strains and displacements are small and continuous, that means the frictions the slips between layers does not exist.
- the displacements have the same order of magnitude as the thickness.
- each layer has the plane stress.

Depending on the plate thickness (h) and displacement order of magnitude (w_z), the stresses can be

negligible in the median plane.

So, for rigid plates ($w_z < 2h$), the strain on *z* direction is considered as being zero and the stresses in the median plane are negligible.

For plates with small displacements ($0.2h < w_z \leq 0.5h$), the deformations in the median plane are taken into account, but the stresses in the median plane are negligible.

For plates with great displacements ($w_z > 0.5h$), the bending displacement are influencing the efforts in median plane.

The FEM delamination analysis rises certain remarks.

- in the case of the displacement variation versus the position of the delamination on the layers, for all three loads, the values of the displacements are approximately equal in perfect case, *c* (plate with delamination oriented at 45^o) and *a* (plate with delamination oriented at 0^o), and *c* (plate with delamination oriented at 90^o);
- it can be observed that in the case of the displacement variation in relation to the delamination position related to the *OX* axis, for all three loads, the displacement values are approximately equal in cases: perfect, *b*, and *a* and *c*.

Due to the fact the delamination existing is decreasing the plate rigidity, the perfect plate displacement is smaller than the plate with delamination.

Experimental tests involve important remarks.

- the difference between FEM model results and experiment results is about 2mm (app. 10%);
- in both cases (numerical and experiments) the same variation of displacements are observed;
- the maximum displacement is greater in *a* and *c* than in cases of perfect plate and *b*. Therefore, the results obtained in cases *a* and *c* can be considered as identical. The same observation in cases perfect plate and *b*.

An important influence of the delamination position on the stresses variation is observed for delaminated plates. As it is seen in Table 12, for perfect plate the normal stress is anti-symmetrical one, while the variation of shear stress is symmetrical one, as are expected.

At the position of laminas where the delamination does exist, this defect significantly changes the internal stress–strain state. It is observed that the stresses have significantly higher values in the case of a cross-section with delamination.

As it is seen, the gap of stresses values for position of embedded delamination at interface between macrolayers is illustrated in Tables 5, 7 and 9, where these values are bolded.

For example, for case *a*, at interface Macrolayer 1 - Macrolayer 2 the σ_x gap is from -88.08 MPa (top) to -8.568 MPa (bottom), and τ_{xy} gap is from -11.89 MPa (top) to -5.03 MPa (bottom).

For case *b*, at interface Macrolayer 1 - Macrolayer 2 the σ_x gap is from -89.4 MPa (top) to -83.52 MPa (bottom), and τ_{xy} gap is from -25.52 MPa (top) to -10.40 MPa (bottom).

For for case *c*, at interface Macrolayer 1 - Macrolayer 2 the σ_x gap is from 145.1 MPa (top) to 23.79 MPa (bottom), and τ_{xy} gap is from 10.17 MPa (top) to 4.119 MPa (bottom).

Important remark: since the sign of τ_{xy} is depending on the related face of stress acting, the sign can be subject of discussing. For the stresses τ_{xy} it is important especially the absolute value.

In Tables 6, 8 and 10 the graphical illustrations of stresses variations are presented. The gap of stresses values (bolded in Tables 5, 7 and 9), are observed.

4. Conclusions

The results of the study show that the performance of the composite laminated imperfect plates is highly dependent on the position and orientation of delamination. The major energy dissipation mechanisms in the delamination process include fiber-matrix debonding, fiber breakage/bridging, microcrack and crack tip plastic deformation.

For FEM calculus validation, a simple evaluating of perfect plate, by using simply supported beam theory in bending has been performed. Taking into account the plate dimensions, the perfect plate has

been modeled as a simply supported beam in bending, loaded by a force on the middle of span. The maximum displacement of the beam model, for each force F_i, is given by the formula $w_i=F_iL^3/48EI$, where L=580 mm (beam span), $F_i=gG_i$ (g=9.81 m/s^2 is gravitational acceleration; $I=bh^3/12$ is sectional moment of inertia; b=100 mm, h=4 mm (sectional dimensions of the equivalent beam). For Young's modulus determination, the Dalton's rule has been used, based on the volumetric ratio of the composite, for E, resulting a value of 19.2 GPa. For each force, the maximum displacement of the equivalent beam is: 10.99 mm; 14.53 mm and 18.07 mm; In FEM analysis these values are: 11.12 mm; 14.69 mm and 18.26 mm, fact which proves that the results of FEM model are validated. Therefore, the models are considered suitable as a basis for investigating the lay-up dependent delamination. According to Figures 5-9 and Tables 6-10, the plate median plane is changing very small due to the existing delamination. Due to the upper discussions, during the layered composite plate design (dimensioning) it is important to include the effects of delamination in the calculation. This aspect would prolong the exploitation period of the laminated structure.

References

1.BIRMAN, V., KARDOMATEAS, G.A., Review of current trends in research and applications of sandwich structures. *Compos Part B-Eng*. **142**, 2018, 221-240.
2BRAGAGNOLO, G., CROCOMBE, A.D., OGIN, S.L., MOHAGHEGHIAN, I., SORDON, A., MEEKS, G., SANTONI, C., Investigation of skin-core debonding in sandwich structures with foam cores. *Mater Design*. **186,** 2020, 1-10.
3.RAMAKRISHNAN, K.V., SUNIL KUMAR G., Applications of sandwich plate system for ship structures. *IOSR j. mech. civ. eng.* 2016, 83-90.
4.BEZNEA, E.F., BAROIU, N., CHIRICĂ, I., The static behavior of a ship deck panel made of composite materials. *Mater Plast*. **58 (4),** 2021, 147-157.
5.ARDHYANANTA, H., SARI, E.N., WICAKSONO, S.T., ISMAIL, H., TUSWAN, T., ISMAIL A., Characterization of vinyl ester bio-resin for core material sandwich panel construction of ship structure application: Effect of palm oil and sesame oil. In AIP Conference Proceedings. **2202,** 2019, 1-5
6.GARG, A., BELARBI, M.O., CHALAK, H.D., CHAKRABARTI, A., A review of the analysis of sandwich FGM structures. *Compos. Struct.* **258,** 2021.
7.AL-SHAMMARI, M.A., ABDULLAH, S.E., Stiffness to weight ratio of various mechanical and thermal loaded hyper composite plate structures, *IOP Conf. Ser. Mater. Sci. Eng.* **433,** 2018.
8.PĂTRAȘCU, A.I., HADĂR, A., PASTRAMĂ, S.D., Structural Analysis of a Freight Wagon with Composite Walls, *Mater. Plast.* **57(2),** 2020, 140-151.
9.KADHIM, A.A., AL-WAILY, M., ALI, Z.A.A.A., JWEEG, M.J., RESAN, K.K., Improvement fatigue life and strength of isotropic hyper composite materials by reinforcement with different powder materials, *Int. J. Mech. Mechatron. Eng*. **18(2),** 2018.
10.NOJAVAN, S., SCHESSER, D., YANG, Q.D., An in situ fatigue-CZM for unified crack initiation and propagation in composites under cyclic loading, *Compos. Struct*. **146,** 2016, 34-49.
11.IMRANA, M., KHANA, R., BADSHAHA, S., Investigating the effect of delamination size, stacking sequences and boundary conditions on the vibration properties of carbon fiber reinforced polymer composite, *Mater. Res.* **22(2),** 2019.
12.DRĂGHICI, S., PĂRĂUȘANU, I., BACIU, F., PETRESCU, H.A., HADĂR, A., PASTRAMĂ, S.D., A Comparative Experimental - Numerical Analysis on the Vibration Behaviour of a Composite Satellite Subset, *Mater. Plast.* **53**(4), 2016, 585-589.
13.ALESADI, A., GALEHDARI, M., SHOJAEE, S., Free vibration and buckling analysis of cross-ply laminated composite plates using Carrera's unified formulation based on Isogeometric approach, *Comput. Struct.* **183,** 2017, 38–47.
14.M. CETKOVIC, Thermal buckling of laminated composite plates using layerwise displacement model, *Compos. Struct.* **142,** 2016, 238–253.

15.BAROIU, N., BEZNEA, E.F., COMAN, G., CHIRICĂ, I., Static and thermal behaviour of ship structure sandwich panels, *Therm. Sci.* **25(A),** 2021, 1109-1121.
16.NEMETH, M.P., Buckling behavior of long anisotropic plates subjected to restrained thermal expansion and mechanical loads, *J. Therm. Stresses*, **23(9),** 2000, 873-916.
17.TELFORD, R., PEETERS, D.M.J., ROUHI, M., WEAVER, P.M., Experimental and numerical study of bending-induced buckling of stiffened composite plate assemblies, *Compos B Eng.* **233,** 2022, 109642.
18.MOITA, J., CORREIA, V.F., SOARES, C.M.M., HERSKOVITS, J., Higher-order finite element models for the static linear and nonlinear behaviour of functionally graded material plate-shell structures, *Compos. Struct*. **212,** 2019, 465–475.
19.GALEȘ, C., BAROIU, N., On the bending of plates in the electromagnetic theory of microstretch elasticity, *ZAMM Z. fur Angew.* **93(1),** 2013, 1–17.
20.ZHU, X., XIONG, C., YIN, J., YIN, D., DENG, H., Bending experiment and mechanical properties analysis of composite sandwich laminated box beams, *Materials.* **12,** 2019, 2959.
21.TAN, C., LI, Y.L., GUO, Y.Z., Mechanical property analysis of composite adhesively bonded sandwich pipe joints. *Acta Mater. Compos. Sin.* **31,** 2014, 1532–1542.
22.LANC, D., TURKALJ, G., PESIC, I., Global buckling analysis model for thin-walled composite laminated beam type structures. *Compos. Struct*. **111,** 2014, 371-380.
23.VO, T.P., LEE, J., Interaction curves for vibration and buckling of thin-walled composite box beams under axial loads and end moments. *Appl. Mathem. Modelling*. **34,** 2010, 3142-3157.
24.SHIN, D., CHOI, S., JANG G.W., KIM, Y.Y., Finite element beam analysis of tapered thin-walled box beams, *Thin-Walled Struct*. **102,** 2016, 205-214.
25.VAN VINH, P., VAN CHINH, N., TOUNSI, A., Static bending and buckling analysis of bi-directional functionally graded porous plates using an improved first-order shear deformation theory and FEM, *Eur. J. Mech. A/Solids*. **96,** 2022, 104743.
26.BELINHA, J., DINIS, L.M.J.S., Analysis of plates and laminates using the element-free Galerkin method, *Comput Struct*. **84,** 2006, 1547–1559.
27.BEZNEA, E.F., CHIRICĂ, I., BAROIU, N., TEODOR, V.G., Parametric study of experimental and numerical simulation of sandwich composite structures flexural behaviour, *Mater. Plast.* **54(4),** 2017, 682-688.
28.TELFORD, R., PEETERS, D.M.J., ROUHI, M., WEAVER, P.M., Experimental and numerical study of bending-induced buckling of stiffened composite plate assemblies. *Compos B Eng*. **233,** 2022, 109642.
29.ZHU, X., XIONG, C., YIN, J., YIN, D., DENG, H., Bending Experiment and mechanical properties analysis of composite sandwich laminated box beams. *Materials*, **12,** 2019, 2959.
30.XUE, J., ZI, L., YUAN, H., LIU, R., Contact analysis for fiber-reinforced, delaminated laminates with kinematic nonlinearity. *Acta Mech. Solida Sin.* **26,** 2013, 388–402.
31.ALSHAHRANI, H., HOJJATI, M., Bending behavior of multilayered textile composite prepregs: Experiment and finite element modeling. *Mater. Des.* **124,** 2017, 211–224.
32.CAVUOTO, R., CUTOLO, A., DAYAL, K., DESERI, L., FRALDI M., Distal and non-symmetrical crack nucleation in delamination of plates via dimensionally-reduced peridynamics, *J. Mech. Phys. Solids*, **172,** 2023, 105189.
33.NASSIRAEI, H., REZADOOST, P., SCFs in tubular X-connections retrofitted with FRP under in-plane bending load, *Compos. Struct.* **274,** 2021, 114314.
34.NASSIRAEI, H., REZADOOST, P., SCFs in tubular X-joints retrofitted with FRP under out-of-plane bending moment, *Mar. Struct.* **79,** 2021, 103010.
35.MALLELA, U.K., UPADHYAY, A., Buckling load prediction of laminated composite stiffened panels subjected to in-plane shear using artificial neural networks, *Thin-Walled Struct.* **102,** 2016, 158-164.

36.SUSAC, F., BEZNEA, E.F., BAROIU, N., Artificial neural network applied to prediction of buckling behavior of the thin walled box, *Adv. Eng. Forum,* **21,** 2016, 141-150.
37.RAKOČEVIĆ, M., ŽUGIĆ, L., A new approach to the embedding of delamination in the layerwise theory of laminated composite plates. *Symmetry*, **14(8),** 2022, 1583.
38.FERREIRA, G.F.O., ALMEIDA JR., J.H.S., RIBEIRO, M.L., FERREIRA, A.J.M., TITA, V., A finite element unified formulation for composite laminates in bending considering progressive damage, *Thin-Walled Struct.* **172,** 2022, 108864.
39.SZEKRÉNYES, A., Differential quadrature solution for composite flat plates with delamination using higher-order layerwise models. *Int. J. Solids Struct.* **248,** 2022, 111621.
40.XUE, J., ZI, L., YUAN, H., LIU, R., Contact analysis for fiber-reinforced, delaminated laminates with kinematic nonlinearity. *Acta Mech. Solida Sin.* **26,** 2013, 388–402.
41.HAGHANI, A., MONDALI, M., FAGHIDIAN, S.A., Linear and nonlinear flexural analysis of higher-order shear deformation laminated plates with circular delamination. *Acta Mech*. **229,** 2018, 1631–1648.
42.JIN, F., XU, P., XIA, F., LIANG, H., YAO, S., XUE, J., Buckling of composite laminates with multiple delaminations: Part I Theoretical and numerical analysis. *Compos. Struct.* **250,** 2020, 112491.
43.KALEEL, I., CARRERA, E., PETROLO, M., Progressive delamination of laminated composites via 1D models, *Compos. Struct.* **235,** 2020, 111799.
44.BRITO-SANTANA, H.,; CHRISTOFF, B.G., FERREIRA, A.J.M., LEBON, F., RODRÍGUEZ-RAMOS, R., TITA, V., Delamination influence on elastic properties of laminated composites, *Acta Mech.* **230,** 2019, 821–837.

Manuscript received: 3.02.2024